Operation Maps for Hybrid Electrolyser and Battery Systems - A Luxembourgish Case Study

Conference Paper · June 2024

DOI: 10.1109/PEDG61800.2024.10667442

6 authors, including:

Ángel Paredes Parrilla
University of Malaga

Jose A Aguado
University of Malaga

Operation Maps for Hybrid Electrolyser and Battery Systems – A Luxembourgish Case Study

Ángel Paredes*, José A. Aguado*, Philipp Fisch†, Patrick Witte†, Sebastian Theissen†, and Pedro Rodríguez‡

*University of Malaga, Dept. of Electrical Engineering, Málaga, Spain, Email: {angelparedes, jaguado}@uma.es
†Green Power Storage Solutions, Wecker, Luxembourg, Email: {philipp.fisch, patrick.witte, sebastian.theissen}@gpss.lu
‡Luxemboug Institute of Science and Technology, Luxembourg, Email: pedro.rodriguez@list.lu

Abstract

The ever-increasing need for climate action motivates the development of new and flexible energy solutions that adapts to society's modern energy requirements. The i-STENTORE project aims to pioneer innovative solutions for the widespread deployment of hybrid energy storage systems. This paper investigates the simultaneous provision of flexibility services and hydrogen production within a real-world Luxembourgish hybrid energy system demonstrator, using multi-objective optimisation. While previous research has focused on either flexibility services or hydrogen production individually, this study fills the gap of a comparative analysis of different scenarios that consider trade-offs between these two objectives. The research provides operational insights into strategies for maximising economic viability and sustainability by analysing aspects such as the levelised cost of hydrogen, energy, degradation, and the impact of the battery size. The results show the potential of this demonstrator to provide flexibility to the system without significantly impacting in the hydrogen production.

Index Terms

Agro-photovoltaics, Battery Energy Storage System, Hydrogen, Multi-objective optimization, Operation Map

NOMENCLATURE

Parameters are in upper case letter and variables in lower case letter. $|\Omega|$ denotes the cardinality of the set Ω.

Indices and sets

t, T Index and set for time periods, $t \in T$.
s, S Index and set for electrolyser operation segments, $s \in S$.
m, M Index and set for the segments of the semi-empirical degradation model, $m \in M$.

Parameters

P^{MAX}, P^{MIN}, P^{SB} Maximum, minimum and standby powers of the electrolyser (kW).
A_s, B_s Coefficients for linearization of hydrogen production in segment s (kg/kW, kg).
$\underline{P}_s, \overline{P}_s$ Minimum and maximum power values in segment s (kW).
a_m, b_m, c_m, d_m Parameters for the semi-empirical degradation model.
η^{CH}, η^{DIS} Charging and discharging efficiencies of the BESS.
P^{CONV} Power rating of the BESS converter (kW).
$\underline{SOC}, \overline{SOC}, SOC0$ Minimum, maximum, and initial state of charge of the BESS (kWh).
$\lambda^{PV}, \lambda^{W}$ Costs of energy acquisition of the APV and WT (€/kWh).
P_t^{PV}, P_t^{WT} Maximum production capacity of the APV and WT at time t (kWh).
r Discount rate.

Variables

$z_t^{ON}, z_t^{OFF}, z_t^{SB}$ Binary variables indicating the ON, OFF and Standby statuses of the electrolyser at timestep t.
$z_{s,t}^{h}$ Binary variable indicating the working segment of the electrolyser s at timestep t.
p_t^{e} Electric power consumption by the electrolyser at timestep t (kW).
$\hat{p}_{s,t}^{e}$ Electric power consumption by the electrolyser at timestep t due to working segment s (kW).
q_t^{h} Produced hydrogen at timestep t (kg).
$\Delta b_{loss,t}^{cal}, \Delta b_{loss,t}^{cyc}$ Calendar and cycle degradation of the BESS at timestep t (kWh).
soc_t State of charge of the BESS at timestep t (kWh).
p_t^{ch}, p_t^{dis} Charging and discharging power of the BESS at timestep t (kW).
$p_t^{r,s}, p_t^{r,e}$ Power from renewables r to BESS s and Electrolyser e at timestep t (kW).

This work was supported by the FPU grant (FPU19/03791) founded by the Spanish Ministry of Education, by Ministerio de Ciencia e Innovación through projects TED2021-132339B-C42 and -C41, by Horizon Europe Programme through projects HORIZON-CL5-2022D3-01 Ref: 101096787, HORIZON-CL5-2022-D4-02-04 Ref: 101123556 and, by the University of Málaga.

$p_t^{s,f}, p_t^{s,e}$ Power from BESS s to flexibility f and Electrolyser e at timestep t (kW).
p_t^{PV}, p_t^{W} Power acquired from APV and WT at timestep t (kW).

I. Introduction

THE global push for climate action has accelerated the need for flexible energy solutions, with energy storage emerging as a key enabler [1]. Despite advancements, challenges remain in cost-effectiveness and operational efficiency, driving initiatives like i-STENTORE to pioneer storage solutions for widespread adoption. The Kielen demonstrator in the i-STENTORE project showcases an application at European level, highlighting how Battery Energy Storage Systems (BESSs) integrated into agro-photovoltaics (APV) farms can optimize renewable energy use and hydrogen production. This innovative approach not only enhances operational efficiency and grid support services but also underscores the potential for hydrogen production within the agricultural sector [2].

Recent research has delved into the advancement of hydrogen-based systems for multple applications. A comprehensive review of hydrogen techno-economic parameters and market dynamics underscores the potential of hydrogen as a key enabler for decarbonization of power applications [3]. Moreover, a discussion of their applicability to stationary and mobile applications has been conducted by [4], highlighting the need for further evaluation of efficiency and economic practicality. Research has also explored the potential of hydrogen-based systems for fostering the decarbonization of the energy sector, emphasizing the need for further capacity in the grid to achieve this objective [5]. In this vein, authors in [6] analysed the potential hydrogen-based systems in Spain, using a tailored energy model to optimize joint renewable and hydrogen strategies towards a low-carbon building stock. Moreover, a techno-economic analysis tool for regional hydrogen hubs demonstrates the effectiveness of hydrogen-based energy storage solutions in reducing the usage of external sources in remote areas [7]. Besides, exploration into optimal hydrogen carriers and transportation concepts for diverse sectors offers insights for storage and transportation [8]. Recent analysis has explored the role of hydrogen in low-carbon electric power systems, emphasizing its importance for hard-to-abate sectors and sector coupling [9]. Furthermore, a techno-economic assessment of hybrid energy flexibility systems for Italian islands' decarbonization highlights the potential of renewable energy integration strategies even in isolated environments [10]. In addition, research suggests that gas switching reforming plants offer flexibility to power systems without reducing the utilization rate of carbon capture and storage infrastructure, thus becoming a key enabling technology for decarbonization led by wind and solar power [11]. Additionally, another study in Baja California, Mexico, showcases the potential of hydrogen-based Power-to-Gas-to-Power systems to reduce CO_2 emissions and contribute to the decarbonization of distributed energy generation [12]. Lastly, This is also confirmed in African contexts, such as in Moroco, where a study of a hybrid microgrid system underscores the potential of hybrid systems to provide cost-effective power to remote communities while mitigating environmental impact [13].

While previous studies have deeply explored the techno-economic potential of hydrogen-based systems, there is a need for further research into the joint optimisation of flexibility services and hydrogen production within a hybrid energy system context. This paper aims to address this gap by conducting a comprehensive evaluation of the multiple objectives of flexibility provision and hydrogen production, shedding light on optimal strategies for maximizing the overall efficiency and sustainability of hybrid energy systems.

The main novelty of this paper is the exploration of the operation maps of a real hybrid system comprised by a BESSs and an electrolyser providing flexibility services and producing hydrogen. The case study is based on a real integration of an APV system, a Wind Turbine (WT), a BESS, and a polymer electrolyte membrane (PEM) electrolyser. The APV system and WT are used to generate renewable energy, which is stored in the BESS and used to produce green hydrogen. The BESS has the potential of providing energy flexibility services to the grid, but a compromise between the hydrogen production and the flexibility services is needed. The results show the ability of the system to provide flexibility without compromising the hydrogen production cost and the degradation of the BESS.

The remainder of this paper is organised as follows. Section II describes the materials and methods used to evaluate the hybrid energy system at hand. Section III presents the results of the case study while Section IV concludes the paper.

II. Material and methods

A schematic of the integrated hybrid energy system is shown in Fig. 1. The APV system and WT are used to generate renewable energy, which is stored in the BESS and used to produce green hydrogen. In this context, the BESS still has room to provide energy flexibility service to the grid, but a precise strategy is needed to avoid jeopardizing the hydrogen production.

A. Hydrogen Production

The electrolyser operates through distinct modes tailored to its varying energy demands and operational states. It features an Off-Mode, where power consumption ceases entirely, ensuring energy efficiency during periods of inactivity. Additionally, it incorporates a Production-Mode, allowing the electrolyser to operate at its nominal power capacity for hydrogen production. A standby mode, known as Hot-Standy, maintains the operating temperature while consuming minimal power, enabling swift

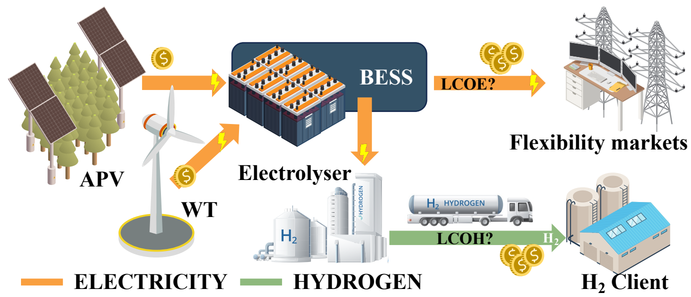

Figure 1. Schematic overview of the integrated hybrid energy system showcasing the interconnection between APV, WT, BESS, and the electrolyser. Two outputs are obtained: flexibility and hydrogen.

transitions to full operation when necessary, as showcased by (1a). To facilitate efficient hydrogen storage and transportation, the system comprises two tanks: a buffer tank positioned after the electrolyser operating at 30 bar pressure, and a high-pressure tank for transportation purposes, maintained at 380 bar pressure.

To model the non-linear efficiency curve a MILP is needed following [14]. Based on the non-linear efficiency curve $\eta(p_E)$ the hydrogen production q_h of the electrolyser is computed using the Higher Heat Value (HHV) of Hydrogen and the electric power input p_E as $q_h = p_E \cdot \eta(p_E)/HHV$. Then, P^{MAX} denote the maximum power rating of the electrolyser as in (1b), defining its upper limit for energy consumption. Similarly, P^{MIN} represents the minimum working power as in (1c), ensuring operational stability during low-demand periods. Coefficients A_s and B_s are utilized for linearizing hydrogen production within different operational segments $s \in S$ in (1d), where S represents the set of segments defining the electrolyser's operational states. P^{SB} denotes the power rating of the standby mode. Variables include binary indicators z_t^{ON}, z_t^{OFF}, and z_t^{SB}, representing the online, offline, and standby statuses of the electrolyser at each time step $t \in T$. Additionally, $z_{s,t}^h$ denotes the working operational segment s at time t in (1e). Note that only one segment is active as (1f) shows. Power-related variables, such as p_t^e in (1g) for electric power consumption and q_t^h for hydrogen production, quantify energy flows within the system over time.

$$z_t^{ON} + z_t^{OFF} + z_t^{SB} = 1 \qquad \forall t \in T \quad (1a)$$
$$p_t^e \leq P^{MAX} z_t^{ON} + P^{SB} z_t^{SB} \qquad \forall t \in T \quad (1b)$$
$$p_t^e \geq P^{MIN} z_t^{ON} + P^{SB} z_t^{SB} \qquad \forall t \in T \quad (1c)$$
$$q_t^h = \sum_{s \in S} (A_s \hat{p}_{s,t}^e + B_s z_{s,t}^h) \qquad \forall t \in T \quad (1d)$$
$$\underline{P}_s z_{s,t}^h \leq \hat{p}_{s,t}^e \leq \overline{P}_s z_{s,t}^h \qquad \forall t \in T, \forall s \in S \quad (1e)$$
$$z_t^{ON} = \sum_{s \in S} z_{s,t}^h \qquad \forall t \in T \quad (1f)$$
$$p_t^e = \sum_{s \in S} \hat{p}_{s,t}^e + P^{SB} z_t^{SB} \qquad \forall t \in T \quad (1g)$$

B. Battery Energy Storage System

The BESS functions as a buffer between renewable energy production, the flexibility services and the electrolyser. This is crucial to be able to couple energy and gas vectors. The state of charge (SOC) of the battery, computed in (2a), bounded by $\underline{SOC}$ and $\overline{SOC}$ in (2c), represents the amount of energy stored within the system at any given time. Charging and discharging of the battery occur through a power converter with efficiencies η^{CH} and η^{DIS}, respectively, ensuring effective energy transfer between the battery and the system. The power rating of the converter, denoted as P^{CONV}, limits the maximum charging or discharging power of the battery in (2d) and (2e).

To address battery degradation, a semi-empirical model is employed to quantify the degradation over time. This model accounts for both calendar and cycle degradation, denoted as $\Delta b_{loss,t}^{cal}$ and $\Delta b_{loss,t}^{cyc}$, respectively. Calendar degradation is influenced by the state of charge (soc_t), while cycle degradation depends on the charging and discharging rates relative to the converter power. These degradation components are represented as non-linear functions discretized into m segments and interpolated as linear functions using parameters a_m, b_m, c_m, and d_m [15], [16]. This will avoid the overuse of the BESS minimising the degradation in the objective while provisioning flexibility and hydrogen. Battery wear is computed as the sum of cycle (2g) and calendar degradation (2f), in (2h).

$$soc_t = soc_{t-1} + \eta^{CH} p_t^{CH} - p_t^{DIS}/\eta^{DIS} \quad \forall t \in T \quad (2a)$$
$$soc_{\|T\|} = SOC0 \quad (2b)$$
$$\underline{SOC} \leq soc_t \leq \overline{SOC} \quad \forall t \in T \quad (2c)$$
$$p_t^{CH} \leq P^{CONV} z_t^{CH} \quad \forall t \in T \quad (2d)$$
$$p_t^{DIS} \leq P^{CONV}(1 - z_t^{CH}) \quad \forall t \in T \quad (2e)$$
$$\Delta b_{loss,t}^{cal} \geq a_m soc_t + b_m \quad \forall m \in M, t \in T \quad (2f)$$
$$\Delta b_{loss,t}^{cyc} \geq c_m (p_t^{ch} - p_t^{dis})/P^{conv} + d_m \quad \forall m \in M, t \in T \quad (2g)$$
$$\Delta b_{loss,t} = \Delta b_{loss,t}^{cal} + \Delta b_{loss,t}^{cyc} \quad \forall t \in T \quad (2h)$$

C. Renewable Energy Management

The interplay of these energy flows is illustrated in Figure 2, depicting the relationships between renewable energy generation, storage, and utilization within the hybrid system.

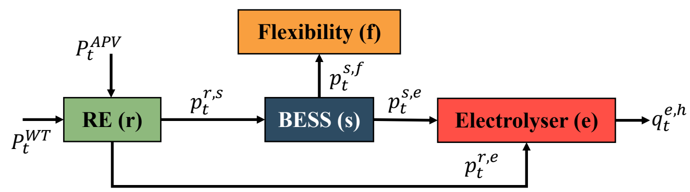

Figure 2. Energy flows in the integrated hybrid system. The energy produced by the APV P_t^{APV} and the WT P_t^{WT} are used to charge the BESS $p_t^{r,s}$ and to produce hydrogen $p_t^{r,e}$. The BESS is used to provide flexibility services $p_t^{s,f}$ and to feed the electrolyser $p_t^{s,e}$. The hydrogen $q_t^{e,h}$ is produced.

The APV system employs a one-axis tracking mechanism to optimize solar energy capture throughout the day. Its operational efficiency relies on the performance of the DC/AC system, which transforms the captured solar energy into usable electricity. The economic viability of utilizing the energy generated by the APV system is determined by the costs of use (€/kWh), guiding decisions on whether to consume the energy locally or sell it in the energy markets. The PV production at time t, denoted as P_t^{PV} (kWh), represents the amount of electricity generated by the APV system, while λ^{PV} (€/kWh) signifies the associated cost.

Similarly, the WT system contributes to renewable energy generation, with its output, P_t^{WT} (kWh), representing the electricity generated by the WT at time t. The costs associated with wind energy production are denoted by λ_t^{W} (€/kWh) and are typically governed by Power Purchase Agreement agreements.

Energy flows within the integrated hybrid system are governed by power balance equations from (3a) to (3d), ensuring operational stability and efficient resource allocation. Power acquired from renewable energy sources, represented by $p_t^{r,s}$ and $p_t^{r,e}$ (kW), is used to charge the BESS and produce hydrogen, respectively. The BESS serves a dual role, providing flexibility services ($p_t^{s,f}$) to the grid and supplying power ($p_t^{s,e}$) to the electrolyser for hydrogen production. Additionally, equations (3e) and (3f) ensure that the energy acquired from the APV and WT systems, p_t^{PV} and p_t^{W}, respectively, does not exceed their respective maximum production capacities at time t, P_t^{PV} and P_t^{WT}, respectively.

$$p_{s,t}^{CH} = p_t^{r,s} \quad \forall t \in T \quad (3a)$$
$$p_{s,t}^{DIS} = p_t^{s,f} + p_t^{s,e} \quad \forall t \in T \quad (3b)$$
$$p_t^{e} + (z_t^{ON} + z_t^{SB}) P^{COMP} = p_t^{r,e} + p_t^{s,e} \quad \forall t \in T \quad (3c)$$
$$p_t^{r,s} + p_t^{r,e} = p_t^{PV} + p_t^{W} \quad \forall t \in T \quad (3d)$$
$$p_t^{PV} \leq P_t^{PV} \quad \forall t \in T \quad (3e)$$
$$p_t^{W} \leq P_t^{WT} \quad \forall t \in T \quad (3f)$$

D. Evaluation of the flexibility potential and H_2 production

The flexibility potential and H_2 production are evaluated using multi-objective optimization. Optimization problems (4a) to (4c) maximize the flexibility potential, the H_2 production, and minimize the degradation of the BESS, respectively.

$$\max \sum_t \left(p_t^{s,f} - \Delta b_{loss,t} \right) \text{ s.t. } (1), (2), (3) \tag{4a}$$

$$\max \sum_t \left(q_t^{e,h} - \Delta b_{loss,t} \right) \text{ s.t. } (1), (2), (3) \tag{4b}$$

$$\min \sum_t \Delta b_{loss,t} \text{ s.t. } (1), (2), (3) \tag{4c}$$

To compute the Pareto front of this multi-objective optimization problem, objectives (4a), and (4b) are successively evaluated using the epsilon-constraint method [17]. The epsilon-constraint method is a technique that allows to compute the relationship among objectives by transforming the problem into a single-objective problem as presented in Algorithm 1, by including the objectives as constraints and solving the problem for different values of ε.

Algorithm 1: Computation of the pareto frontier

begin
    $\overline{P}^f, \overline{Q}^{H_2} \leftarrow \arg\max\,(4a), \arg\max\,(4b)$
    $\varepsilon \leftarrow 0$
    while $\varepsilon \leq 1$ **do**
        $P^f(\varepsilon), Q^{H_2}(\varepsilon) \leftarrow \arg\,(4b) \text{ s.t. } \sum_t p_t^{s,f} \geq \overline{P}^f \varepsilon$
        $\varepsilon \leftarrow \varepsilon + \Delta\varepsilon$
    end
end

Then, after obtaining the Pareto front using the Algorithm 1, the operation map is computed as presented in Algorithm 2 using objective (4c) and including minimum flexibility and hydrogen production constraints into the problem.

Algorithm 2: Computation of operation map

begin
    $\overline{P}^f, \overline{Q}^{H_2}, P^f(\varepsilon), Q^{H_2}(\varepsilon) \leftarrow$ Algorithm 1
    $\varepsilon, \mu \leftarrow 0$
    while $\varepsilon \leq 1$ **do**
        while $\mu \leq 1$ **do**
            $P^f(\varepsilon, \mu), Q^{H_2}(\varepsilon, \mu) \leftarrow \arg\min\,(4c) \text{ s.t. } \sum_t p_t^{s,f} \geq \overline{P}^f \varepsilon, \sum_t q_t^{e,h} \geq \overline{Q}^{H_2}(\varepsilon)\mu$
            $\mu \leftarrow \mu + \Delta\mu$
        end
        $\varepsilon \leftarrow \varepsilon + \Delta\varepsilon$
    end
end

For each point of the obtained Pareto-optimal solutions, the operation map is computed. This operation map shows the total degradation of the battery $\Delta b_{loss,t}$, the levelised cost of energy (LCOE) for the flexibility provision and the levelised cost of the hydrogen (LCOH), for each point of the Pareto-optimal solutions. The LCOE and LCOH are computed in (5a) and (5b) following [18], [19].

$$LCOH = \sum_t \frac{C_t^I + C_t^E + C_t^M}{(1+r)^t} \Big/ \sum_t \frac{Q_t^{H_2}}{(1+r)^t} \tag{5a}$$

$$LCOE = \sum_t \frac{C_t^I + C_t^E + C_t^M}{(1+r)^t} \Big/ \sum_t \frac{P_t^f}{(1+r)^t} \tag{5b}$$

where C_t^I, C_t^E, and C_t^M are the investment, energy, and maintenance costs at time t, respectively, $Q_t^{H_2}$ is the hydrogen production at time t, and P_t^f is the flexibility production at year t, and r is the discount rate.

III. Results and discussions

A. System and Scenario Description

The integrated energy system encompasses an APV plant, a WT, a utility-scale BESS, and a PEM electrolyser for green hydrogen production. The APV plant, with 4 MWp installed capacity and an annual yield of 6.8 GWh, forms the primary renewable energy source. The WT, with 4.2 MW installed power and an annual yield exceeding 10 GWh, complements the APV's generation capacity. The BESS, rated at 1 MW/1MWh and equipped with grid-forming capabilities, serves to optimize energy utilization, enhance grid stability, and offer ancillary services to the distribution grid. Additionally, the PEM electrolyser, with a rated power of 1 MW and an annual hydrogen production potential of up to 164,000 kg, facilitates green hydrogen production, the configuration of the site is presented in Fig. 3.

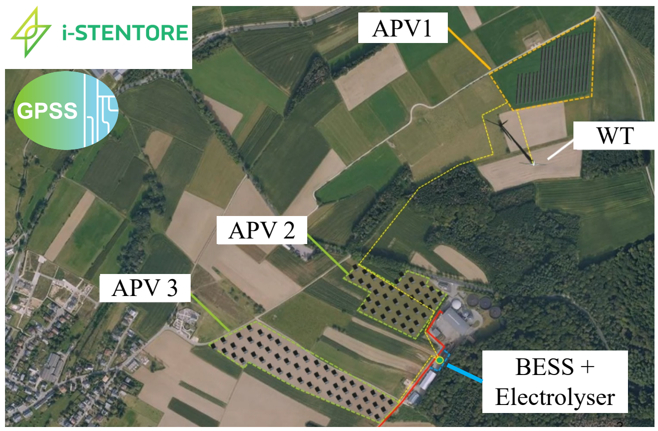

Figure 3. GPSS facility for the case study at hand. There exist three diferent APV farms and one WT. The BESS and the Electrolyser are located in the same site.

The efficiency curve is approximated using a piecewise linear approximation of the hydrogen production as Fig. 4 shows, considering an HHV of 39.39 kWh/kg. In a similar vein, BESS degradation parameters a_m, b_m, c_m, and d_m are obtained from the manufacturer's data sheet.

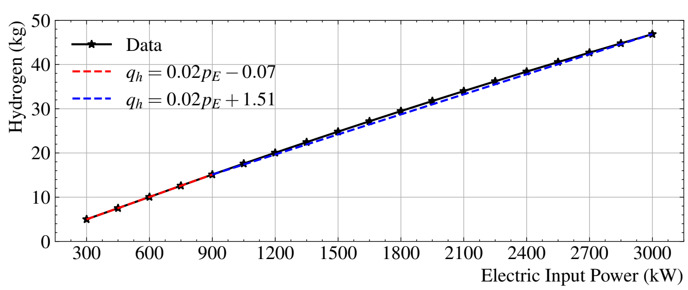

Figure 4. Hydrogen production curve of the electrolyser. The curve is approximated using a piecewise linear approximation of the hydrogen production.

To evaluate the system's performance, renewable energy profiles are obtained from historical data [20], [21]. Simulations are performed using Gurobi 10.0.3 and Python 3.11.4 on an Apple M1 Processor with 16 GB of RAM. The simulation considers an hourly time resolution for a year (8760 time steps), the total number of continuous variables is 131,401, the number of binary variables is 52,560 and the total number of constraints is 367,922. The solver takes approximately 791 seconds to solve each problem considering a MIP gap of 5%.

B. Operation Maps and Pareto Frontier

Figures 5, 6, and 7 show the results of the multi-objective optimization. The operation map in Fig. 5 shows the total degradation of the battery for a year of operation. The LCOE map in Fig. 6 shows the LCOE for the provision of flexibility services. The LCOH map in Fig. 7 shows the LCOH for the hydrogen production. As the results show, the system is able to provide inexpensive flexibility services and produce hydrogen at a low cost. Fig. 6 shows that the LCOE contour lines are slightly tilted towards the flexibility provision, indicating minor increase in the LCOE as the hydrogen production increase. Whereas the LCOH contour lines are completely horizontal, indicating that the LCOH is not affected by the flexibility provision.

This is due to the fact that the BESS is able to provide flexibility services without compromising the hydrogen production cost and the degradation of the BESS. This could also be shown in the Pareto frontier being near rectangular, indicating that the trade-offs between the flexibility provision and the hydrogen production are minimal.

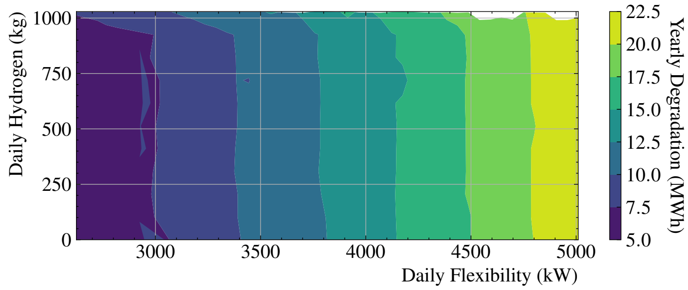

Figure 5. Operation map of the integrated hybrid energy system showcasing the total degradation of the battery for a year of operation.

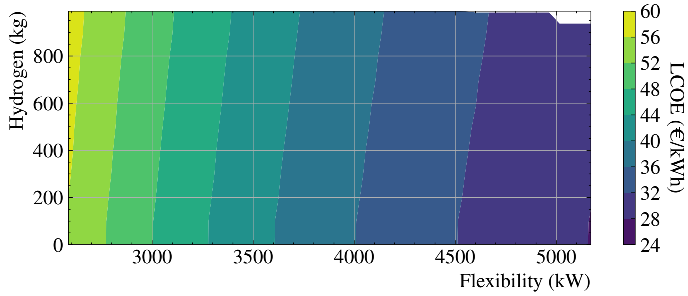

Figure 6. Operation map of the integrated hybrid energy system showcasing the LCOE for the provision of flexibility services.

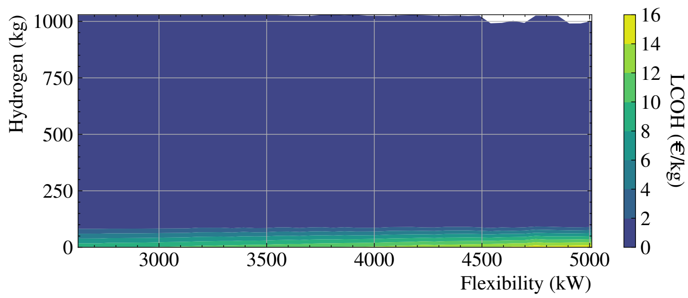

Figure 7. Operation map of the integrated hybrid energy system showcasing the LCOH for the hydrogen production.

C. Effect of the BESS size

To evaluate the effect of the BESS size on the operation of the system, the LCOE and LCOH are computed for different BESS sizes when the system maximise both the flexibility provision and the hydrogen production. The results are shown in Fig. 8 for values of BESS Capacity from 1 MWh to 10 MWh considering ratios of 1:0.5, 1:1, 1:1.5, and 1:2 for the energy capacity and power rating of the BESS. As shown, the LCOE asyntotically decrease with the BESS size up to 80%, while the LCOH exhibits a linear increase with it. This is due to the fact that the BESS is able to provide more flexibility services and store more energy from the renewables, but the hydrogen production is limited by the electrolyser power rating.

Regarding the BESS power rating, there is a big difference in the LCOE and LCOH when going from a 1:0.5 to a 1:1 ratio, but the difference is minimal when going from a 1:1 to a 1:2 ratio. In the case of the LCOE, bigger BESS power ratings are able to fully capture the energy from the renewables, reducing the LCOE up to 40%. In the case of the LCOH, the BESS power rating does the opposite effect, increasing the LCOH up to 25% when going from a 1:0.5 to a 1:1 ratio, this is due to the limited power rating of the electrolyser.

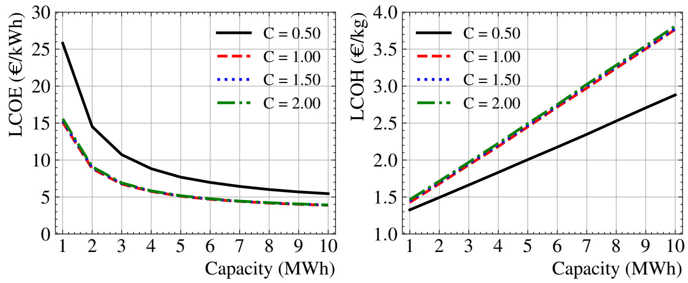

Figure 8. Effect of the BESS size on the LCOE and LCOH when the system maximise both the flexibility provision and the hydrogen production.

IV. Conclusion

This paper addresses the critical need for flexible energy solutions and green hydrogen production in the context of climate action. By integrating BESSs and PEM electrolyser, it demonstrates a pioneering approach to maximizing renewable energy utilization and hydrogen production. The Kielen demonstrator, as part of the i-STENTORE project, exemplifies the potential for such systems at European level, particularly within the agricultural sector. Through the degradation, LCOE and LCOH operation maps, the study reveals the system's ability to provide both flexibility services to the grid and cost-effective hydrogen production without compromising operational efficiency. The presented operation maps and Pareto frontier highlight the balance between flexibility provision, hydrogen production, and BESS degradation, showcasing the system's robustness and potential for widespread adoption in decarbonizing energy systems. It was also shown that the BESS size has a significant impact on the operation of the system, achieving LCOE reductions up to 80%, but could double the LCOH if the electrolyser rating is small, as for this case. This research underscores the significance of joint optimisation in enhancing the efficiency and sustainability of hybrid energy systems, contributing to the advancement of renewable energy technologies and climate mitigation efforts.

References

[1] International Renewable Energy Agency (IRENA), "Electricity storage and renewables: Costs and markets to 2030," p. 132, 2017.
[2] European Dynamics Luxembourg. (2022) innovative Energy Storage TEchnologies TOwards increased Renewables integration and Efficient Operation.
[3] V. M. Maestre, A. Ortiz, and I. Ortiz, "Challenges and prospects of renewable hydrogen-based strategies for full decarbonization of stationary power applications," *Renew. Sustain. Energy Rev.*, vol. 152, p. 111628, 2021.
[4] I. A. Hassan, H. S. Ramadan, M. A. Saleh, and D. Hissel, "Hydrogen storage technologies for stationary and mobile applications: Review, analysis and perspectives," *Renew. Sustain. Energy Rev.*, vol. 149, no. June, p. 111311, 2021.
[5] A. M. Alonso, D. Costa, M. Messagie, and T. Coosemans, "Techno-economic assessment on hybrid energy storage systems comprising hydrogen and batteries: A case study in Belgium," *Int. J. Hydrogen Energy*, vol. 52, pp. 1124–1135, 2024.
[6] V. M. Maestre, A. Ortiz, and I. Ortiz, "Transition to a low-carbon building stock. Techno-economic and spatial optimization of renewables-hydrogen strategies in Spain," *J. Energy Storage*, vol. 56, no. October, 2022.
[7] C. Moran, E. Moylan, J. Reardon, T. A. Gunawan, P. Deane, S. Yousefian, and R. F. Monaghan, "A flexible techno-economic analysis tool for regional hydrogen hubs – A case study for Ireland," *Int. J. Hydrogen Energy*, vol. 48, no. 74, pp. 28 649–28 667, 2023.
[8] M. Otto, K. L. Chagoya, R. G. Blair, S. M. Hick, and J. S. Kapat, "Optimal hydrogen carrier: Holistic evaluation of hydrogen storage and transportation concepts for power generation, aviation, and transportation," *J. Energy Storage*, vol. 55, no. PD, p. 105714, 2022.
[9] M. Schulthoff, I. Rudnick, A. Bose, and E. Gençer, "Role of Hydrogen in a Low-Carbon Electric Power System: A Case Study," *Front. Energy Res.*, vol. 8, no. January, pp. 1–13, 2021.
[10] S. Hoseinzadeh and D. Astiaso Garcia, "Techno-economic assessment of hybrid energy flexibility systems for islands' decarbonization: A case study in Italy," *Sustain. Energy Technol. Assessments*, vol. 51, no. December 2021, p. 101929, 2022.
[11] S. Cloete and L. Hirth, "Flexible power and hydrogen production: Finding synergy between CCS and variable renewables," *Energy*, vol. 192, p. 116671, 2020.
[12] J. de la Cruz-Soto, I. Azkona-Bedia, N. Velazquez-Limon, and T. Romero-Castanon, "A techno-economic study for a hydrogen storage system in a microgrid located in baja California, Mexico. Levelized cost of energy for power to gas to power scenarios," *Int. J. Hydrogen Energy*, vol. 47, no. 70, pp. 30 050–30 061, 2022.
[13] S. El Hassani, F. Oueslati, O. Horma, D. Santana, M. A. Moussaoui, and A. Mezrhab, "Techno-economic feasibility and performance analysis of an islanded hybrid renewable energy system with hydrogen storage in Morocco," *J. Energy Storage*, vol. 68, no. June, p. 107853, 2023.
[14] M. T. Baumhof, E. Raheli, A. G. Johnsen, and J. Kazempour, "Optimization of hybrid power plants: When is a detailed electrolyzer model necessary?" in *2023 IEEE Belgrade PowerTech*, 2023, pp. 1–10.
[15] N. Collath, B. Tepe, S. Englberger, A. Jossen, and H. Hesse, "Aging aware operation of lithium-ion battery energy storage systems: A review," *J. Energy Storage*, vol. 55, no. PC, p. 105634, 2022.
[16] M. A. Ortega-Vazquez, "Optimal scheduling of electric vehicle charging and vehicle-to-grid services at household level including battery degradation and price uncertainty," *IET Gener. Transm. Distrib.*, vol. 8, no. 6, pp. 1007–1016, 2014.
[17] J. Li, J. Chen, Z. Yuan, L. Xu, Y. Zhang, and M. Al-Bahrani, "Multi-objective risk-constrained optimal performance of hydrogen-based multi energy systems for future sustainable societies," *Sustain. Cities Soc.*, vol. 87, no. September, 2022.
[18] F. Nigbur, M. Robinius, and M. Deutsch, "Levelised cost of hydrogen," *Agora Ind. Agora Energiewende*, no. July, 2023.
[19] T. A. Gunawan, A. Singlitico, P. Blount, J. G. Carton, and R. F. Monaghan, "Towards techno-economic evaluation of renewable hydrogen production from wind curtailment and injection into the Irish gas network," *ECOS 2019 - Proc. 32nd Int. Conf. Effic. Cost, Optim. Simul. Environ. Impact Energy Syst.*, pp. 1103–1119, 2019.
[20] S. Pfenninger and I. Staffell, "Long-term patterns of european pv output using 30 years of validated hourly reanalysis and satellite data," *Energy*, vol. 114, p. 1251–1265, Nov. 2016.

[21] I. Staffell and S. Pfenninger, “Using bias-corrected reanalysis to simulate current and future wind power output,” *Energy*, vol. 114, p. 1224–1239, Nov. 2016.